

A Numerical Study of Low Reynolds Unsteady Aerodynamics of a Corrugated Wing

低レイノルズ数流れ場におけるコルゲート翼の非定常空力特性の数値的検証

Yoh MURAKAMI, Yasutada TANABE and Shigeru SAITO (JAXA)

and

Hideaki SUGAWARA (Ryoyu Systems Co., Ltd., Nagoya, Japan)

ABSTRACT

This paper is related to a two-dimensional numerical study about aerodynamic properties of airfoils in low Reynolds number flows. Four types of airfoils including a corrugated wing were selected for the computation and their aerodynamic features against both stationary and dynamic flow cases were examined. Even in a steady flow, there can generally be small unsteady fluctuations in aerodynamic coefficients, and it was identified that the corrugated wing alone exhibits a remarkable stability against such fluctuations. In the dynamic cases, the airfoils were given either heaving motion alone or heaving in combination with feathering motion. Results from the heaving case show that the corrugated wing yields the smallest fluctuations in drag and moment coefficients, indicating its being most stable among four. Results from heaving in combination with feathering case do not underline any apparent superiority of the corrugated wing to others but its characteristic behaviour was highlighted.

1.0 INTRODUCTION

Flying machines have continuously been becoming faster and larger throughout its history, and the remarkable development achieved in the twentieth century rapidly and intensively fostered the field of high Reynolds number aerodynamics. In the mean while, however, low Reynolds number flows have attracted only scant attention from aerodynamicists, in part because low Reynolds number flows had long been considered to have little to do with practical aircraft. Still, recent rapid development in electronics and nanotechnology opened up the possibility to fly tiny and considerably slow flying machines. In point of fact, the U.S. Defense Advanced Research Projects Agency (DARPA) started investigating the possibility of practically building micro air vehicles (MAVs) for many civilian purposes such as surveillance, bio-chemical sensing, atmospheric sampling and so on, as well as military applications, already in the 1990s. Other countries including the U.K., France, Israel, Italy, Russia, Turkey, China and Japan followed the States in rather a parallel manner, some of whose MAVs are about to be put in practical use. DARPA recently launched a new project of even smaller vehicles called 'nano air vehicles' (NAVs) that does not exceed 75 mm in any dimension. Also, recent projects of exploring Mars including EMM (European Mars Mission) ushered research interests in low Reynolds aerodynamics since Mars ascent vehicles (also often shortened as MAVs) are expected to operate in low Reynolds number flows under the thin Martian atmosphere and the weak gravity. Although MAVs hugely vary in the size and configuration, one of most promising methods for flying MAVs is arguably using insect-like flapping wings, especially for extremely small MAVs, from the aerodynamic point of view. Low Reynolds

number aerodynamics with regard to flapping flying objects thus started to attract growing interests, not only from zoologists who are interested in insects from a bio-kinematic point of view, but also from aerodynamicists who are engaged in small MAV projects. Still, theoretical studies in this field have not yet formed a sound basis to back up experimental studies, partly because precedent studies about insects conducted by zoologists were focused more on biological aspects than on theoretical aerodynamics. The present study numerically simulates air flows around heaving wings with a particular aim to focus on a corrugated wing, which is typical of dragonflies, as that zigzag-shaped airfoil reportedly behaves quite differently from conventional airfoils. The specific wing section of the corrugated wing used in this study was reproduced from Obata's experimental work^[1] with his permission and the test cases simulated were determined following Okamoto and Azuma's experimental study^[2], with an aim to later correlate the numerical results with their experimental data. Together with the corrugated wing section, flat plate, circular arc blades with the camber of 4% and 9% were simulated under the same conditions in order to compare their aerodynamic properties. Note that the scope of this study shall not be limited only to insect-like flapping vehicles, because the insight into unsteady low-Reynolds number aerodynamics must be of great value for rotary-winged MAVs as well. It is also worth mentioning here that the autogyro is now seriously studied as a promising configuration to softly land on Mars as a EMM projects. Low-Reynolds number aerodynamics has thus recently been attracting increasing interests from rotorcraft engineers too. The details of the computational method will be enunciated in the next section.

2.0 NUMERICAL SIMULATION

The numerical code used in this study is named rFlow2D, which is a Navier-Stokes solver based on the overlapping grid method. This code was originally developed by Y. Tanabe of JAXA[3] for simulating air flows around a helicopter rotor. The governing equations of flow in this code are represented as follows:

$$\frac{\partial \mathbf{Q}}{\partial t} + \frac{\partial}{\partial x} \left(\mathbf{E} - \frac{\mathbf{E}_v}{\text{Re}} \right) + \frac{\partial}{\partial y} \left(\mathbf{F} - \frac{\mathbf{F}_v}{\text{Re}} \right) = \mathbf{0}, \quad (1)$$

$$\mathbf{Q} = \begin{pmatrix} \rho \\ \rho u \\ \rho v \\ e \end{pmatrix}, \quad \mathbf{E} = \begin{pmatrix} \rho u \\ \rho u^2 + P \\ \rho uv \\ u(e+P) \end{pmatrix}, \quad \mathbf{F} = \begin{pmatrix} \rho v \\ \rho uv \\ \rho v^2 + P \\ v(e+P) \end{pmatrix}, \quad \mathbf{E}_v = \begin{pmatrix} 0 \\ \tau_{xx} \\ \tau_{xy} \\ \beta_x \end{pmatrix}, \quad \mathbf{F}_v = \begin{pmatrix} 0 \\ \tau_{xy} \\ \tau_{yy} \\ \beta_y \end{pmatrix}, \quad (2)$$

where vector \mathbf{Q} represents the flow, \mathbf{E} and \mathbf{F} are inviscid flux vectors for x- and y-directions respectively, \mathbf{E}_v and \mathbf{F}_v are viscous flux vectors for x- and y-directions respectively, ρ is air density, P is pressure, e is specific total energy density and Re is Reynolds number. Note that a perfect gas satisfies a relation known as the equation of state, $P = \rho(\gamma - 1)(e - (1/2)(u^2 + v^2))$, in which the ratio of specific heats, γ , is 1.40 for dry air, and hence the speed of sound, c , can be obtained from the equation of state as $c = \sqrt{\gamma P / \rho}$. This numerical code can conduct time-marching simulation by a dual-time stepping method, using either the LUSGS (Lower-Upper Symmetric Gauss-Seidel) method or DP-LUR (Data-Parallel Lower-Upper Relaxation) method. The FCMT (Fourth-order Compact MUSCL TVD) interpolation method, and the bi-linear interpolation is used for data exchange between overlapped grids. Consequently, rFlow2D ensures a fourth-order spatial resolution, with the favorable TVD (Total Variations Diminishing) property unimpaired.

It is worth noting here that the mSLAU scheme[4] (modified SLAU scheme) is implemented in rFlow2D to solve the non-linear term in Eq. (1) for handling low speed flows, whose Mach number can be as low as 0.01, on top of the ability of solving high speed flows where $M > 1$. SLAU is an AUSM (Advection Upstream Splitting Method)-type scheme, in which the numerical flux in Eq. (1) is described as

$$\bar{\mathbf{F}} = \frac{\hat{m}^+ |\hat{m}|}{2} \mathbf{\Phi}^L + \frac{\hat{m}^- |\hat{m}|}{2} \mathbf{\Phi}^R + \bar{P} \mathbf{N}, \quad (3)$$

where \hat{m} and \bar{P} are the mass flux and pressure defined on the surface of a cell. Note that the superscripts of L and R denote the left (upstream) and right (downstream) boundaries of a cell, respectively. Vectors $\mathbf{\Phi}$ and \mathbf{N} are defined as

$$\mathbf{\Phi} = (1, u, v, h)', \quad \mathbf{N} = (0, x_n, y_n, v_n)', \quad (4)$$

where u and v are flow speed components in the

x- and y-directions respectively, x_n and y_n are unit normal vectors and v_n is the normal component of the speed of a reference moving grid. Note that $h = (e + P) / \rho$ and $v_n = x_n \dot{x} + y_n \dot{y}$. Other relevant variables are defined as follows:

$$\bar{P} = \frac{P^L + P^R}{2} + \frac{\beta^+ - \beta^-}{2} (P^L - P^R) + (1 - \chi) (\beta^+ + \beta^- - 1) \frac{P^L + P^R}{2}, \quad (5)$$

$$M^+ = \frac{V_n^L - v_n}{\bar{c}}, \quad M^- = \frac{V_n^R - v_n}{\bar{c}}, \quad V_n = x_n u + y_n v, \quad (6)$$

$$\chi = (1 - \hat{M})^2, \quad (7)$$

$$\beta^\pm = \begin{cases} \frac{1}{4} (2 \mp M^\pm) (M^\pm \pm 1)^2 & \text{for } |M^\pm| < 1 \\ \frac{1}{2} (1 + \text{sgn}(\pm M^\pm)) & \text{otherwise,} \end{cases} \quad (8)$$

$$\hat{M} = \min \left[1.0, \frac{1}{\bar{c}} \sqrt{\frac{(V_n^L - v_n)^2 + (V_n^R - v_n)^2}{2}} \right], \quad (9)$$

where \bar{c} is the arithmetic mean value of the speed of sound defined at a cell as $\bar{c} = (1/2)(c^L + c^R)$.

It is characteristic with the SLAU scheme that pressure is described as such a function of the Mach number that it depends on the advection speed in a low Mach number region, while it is dominated by the speed of sound in a high Mach number region. M^\pm and \hat{M} in mSLAU are modified from the original SLAU scheme so as to be fit in the moving overlapping grid method. The mass flux is defined as

$$\hat{m} = \frac{1}{2} \left\{ \rho^L (V_n^L + |\bar{V}_n|^+) + \rho^R (V_n^R - |\bar{V}_n|^-) - \frac{\chi}{\bar{c}} \Delta P \right\}, \quad (11)$$

$$\text{where } |\bar{V}_n|^{\pm} = (1 - g) |\bar{V}_n|^+ + g |\bar{V}_n|^-, \quad (12)$$

$$g = -\max(\min(M^+, 0), -1) \times \min(\max(M^-, 0), 1), \quad (13)$$

$$|\bar{V}_n|^{\pm} = \frac{\rho^L |\bar{V}_n|^+ + \rho^R |\bar{V}_n|^-}{\rho^L + \rho^R}, \quad (14)$$

$$\Delta P = P^R - P^L. \quad (15)$$

Four types of airfoils, i.e., flat plate, circular arc blades with the camber of 4% and 9% and a corrugated wing, which is modeled after a type of dragonfly (anax parthenope) in Obata's experimental study^[1] (Fig. 1), are numerically examined for each of the following six cases (case numbers shall be cited later to refer to each test case);

1. steady flow ($\text{Re} = 2000$) around a stationary wing,
2. steady flow ($\text{Re} = 7600$) around a stationary wing,
3. steady flow ($\text{Re} = 2400$) around a heaving wing,
4. steady flow ($\text{Re} = 7600$) around a heaving wing,
5. steady flow ($\text{Re} = 2400$) around a heaving and feathering wing,

6. steady flow ($Re = 7600$) around a heaving and feathering wing.

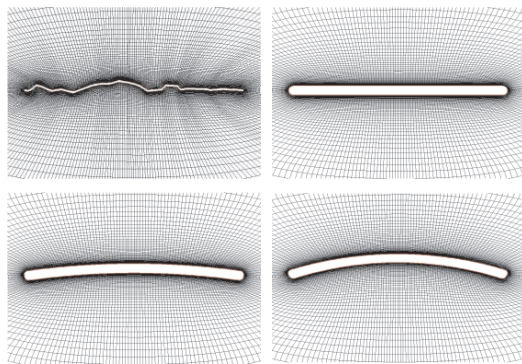


Fig. 1 Tested Airfoils, corrugated wing (top left), flat plate (top right), 4% arc blade (left below) and 9% arc blade (right below)

The wing chord length is non-dimensionalised as the unit in the computation, and the moving inner grid system (flow field in the vicinity of a wing) is discretised into circa 14,000 grids on top of the outer back ground grid system which has circa 40,000 grids over the area of 31×31 . The Mach number of the steady flow is retained as 0.1 throughout the present study.

3.0 RESULTS

3.1 Steady Flow around Stationary Wings

All of four airfoils are put in a steady flow when $M = 0.1$ with angles of attack, α , ranging from -20° to 20° for either $Re = 2000$ or $Re = 7600$. Diagrams and tables below summarise the aerodynamic properties of the wings. Note that the corrugated wing is designated as DGF in the diagrams and tables.

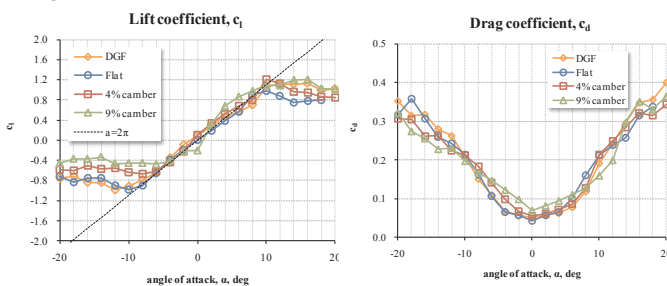


Fig. 2 (left) Lift coefficient ($Re = 2000$), Fig. 3 (right) Drag coefficient ($Re = 2000$)

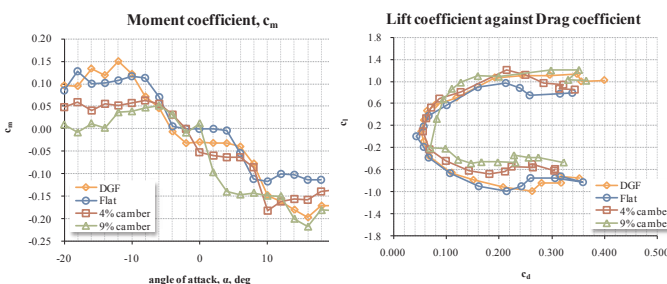


Fig. 4 (left) Moment coefficients ($Re = 2000$), Fig. 5 (right) Lift against drag ($Re = 2000$)

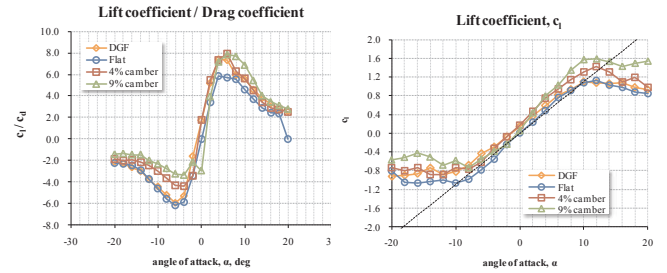
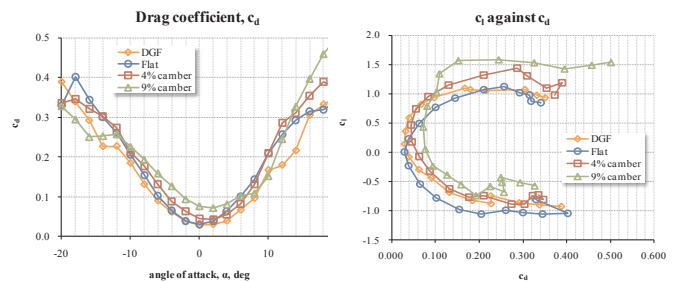


Fig. 6 (left) Lift-drag ratio ($Re = 2000$), Fig. 7 (right) Lift coefficient ($Re = 7600$)

	c_{lmax}	c_{dmax}	$(c_l/c_d)_{max}$
Flat plate	0.977	0.052	7.41
4% Arc	1.206	0.043	5.83
9% Arc	1.210	0.056	7.91
DGF	1.128	0.070	7.86

Table 1 Maximum coefficients ($Re = 2000$)

Fig. 8 (left) Drag coefficient ($Re = 7600$), Fig. 9 (right) Lift against drag ($Re = 7600$)

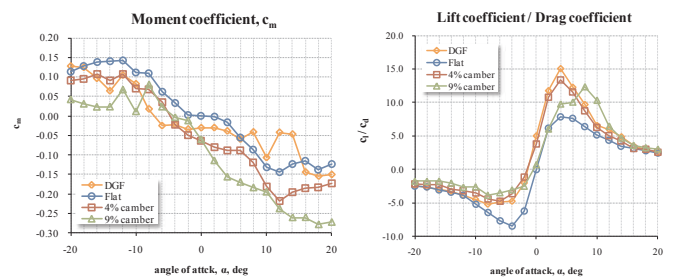


against drag ($Re = 7600$)

	c_{lmax}	c_{dmax}	$(c_l/c_d)_{max}$
Flat plate	1.124	0.402	7.85
4% Arc	1.432	0.389	13.34
9% Arc	1.583	0.502	12.31
DGF	1.099	0.388	15.11

Table 2 Maximum coefficients ($Re = 7600$)

Fig. 10 (left) Moment coefficient ($Re = 7600$), Fig. 11 (right) Lift-drag ratio ($Re = 7600$)



Lift-drag ratio ($Re = 7600$)

With regard to these time-averaged aerodynamic coefficients, the simulational results may indicate that the general qualitative tendencies of the four wings are apparently similar, and none of them appears crucially superior to other three. Still, with regard to unsteady small fluctuations, which are filtered out in the averaged values, it

was identified in the time-histories of those coefficients that the corrugated wing behaves markedly differently from others. Some examples of the fluctuations seen in lift coefficient are to be shown in the following diagrams for $Re = 2000$.

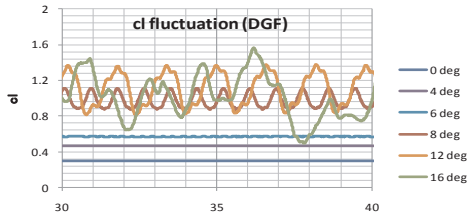


Fig. 12 Fluctuation in c_l of 9% arc blade ($\alpha = 0^\circ, \alpha = 8^\circ, \alpha = 16^\circ, Re = 2000$)

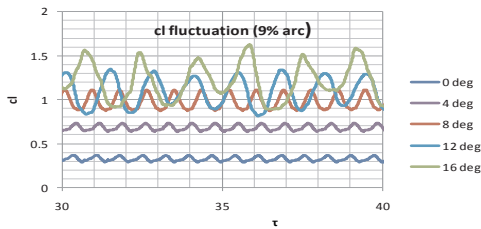


Fig. 13 Fluctuation in c_l of DGF ($\alpha = 0^\circ$ (left), $\alpha = 8^\circ$ (middle), $\alpha = 16^\circ$ (right), $Re = 2000$)

Compared to the 9% arc blade that shows restless fluctuations in lift coefficient, the corrugated wing shows almost constant values for angles of attack of $0^\circ, 4^\circ$ and 6° , though tiny fluctuations are recognizable for 6° in the diagram. Even the corrugated wing starts showing fluctuations at about $\alpha = 8^\circ$ or larger, arguably due to the stall.

The flat plate and the 4% arc blade behave much in the same manner as the 9% arc blade does, albeit with slightly smaller amplitudes. Also, even when $Re = 7600$, it was confirmed that the corrugated wing is much more stable than other wings against the unsteady fluctuation. Considering the fact that a major cause for the fluctuation is vortices which are almost rhythmically released from the wing one after another^[5], the corrugated wing can be considered to have a distinctive feature to stably capture vortices on its surface. This theory can be strengthened by Figs. 14 and 15 that show that the corrugated wing is trapping vortices (coloured in black) well into rumples on the wing surface, resulting in forming neatly slicked streamlines thereabouts. It is worth noting here that streamlines in Figs. 14 and 15 closely resemble Obata's experimental results in Ref. [1].

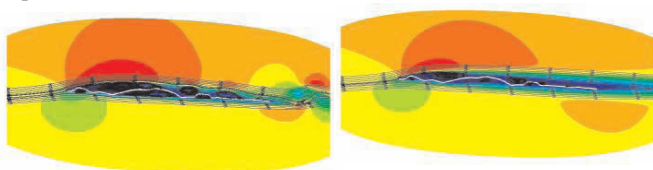


Fig. 14 (left) Streamlines around DGF ($Re = 2400$),
Fig. 15 (right) Streamlines around DGF ($Re = 7600$)

3.2 Steady Flow around Heaving Wings

All of the four airfoils are put in a steady flow with heaving motion. Note that the instantaneous angle of attack of a wing should be defined as follows.

$$\alpha = \theta + \phi, \quad \phi = \arctan(\dot{h}/V) \quad (16)$$

where θ is feathering angle, h is the heaving displacement and V is the inflow velocity. In this case, the feathering angle is fixed at 6° , the amplitude of the heaving motion is 0.5 and the reduced frequency, defined as $k = c\omega/2V$, is 0.31 following Ref. [2].

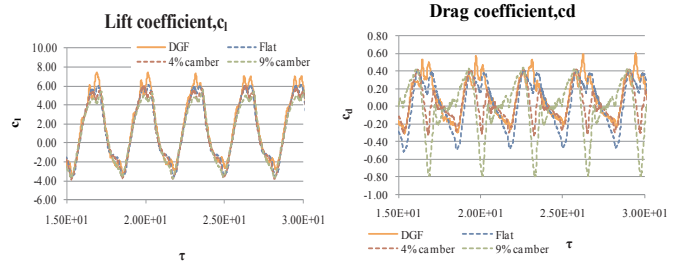


Fig. 16 (left) Lift coefficient ($Re = 2400$), **Fig. 17 (right) Drag coefficient** ($Re = 2400$)

	c_l	c_d	c_m
DGF	1.726	0.110	-0.289
Flat plate	1.351	0.040	-0.274
4% Arc	1.302	0.018	-0.284
9% Arc	1.129	-0.016	-0.241

Table 3 Mean values of c_l, c_d and c_m ($Re = 2400$)

While the four wings exhibit almost the same lift coefficients that alter together with the heaving motion, substantial differences can be seen in drag and moment coefficients; with regard to drag coefficients, 4% and 9% arc blades behave almost in the same way only with different amplitudes, while the flat plate lags in reaching peaks by almost 180° . With regard to moment coefficients, those of flat plate, 4% and 9% arc blades nearly coincide. The corrugated wing, on the other hand, shows considerably different behaviour in terms of both the amplitude and the phase. It is particularly interesting that whereas the corrugated wing exhibits the largest lift, it still shows the smallest deviations in both drag and moment coefficients, viz., it is arguably most efficient and stable during the heaving motion. The same simulation was carried out for $Re = 7600$ and it was confirmed that the wings behave much in the same way as for $Re = 2400$, qualitatively. The results thereof shall thus be herein left out for want of space of paper.

3.3 Steady Flow around Heaving and Feathering Wings

In this case, heaving and feathering motions are both taken into consideration at a time. The heaving

displacement is described as $h = 0.5c \sin(kt + \pi/2)$ and the feathering motion is provided as $\theta = \theta_0 + (0.5ck/V) \sin(kt)$ so that the instantaneous angle of attach of the wing should be retained constant. The amplitude of the feathering motion, i.e. $(0.5ck/V)$, becomes circa 17.76° .

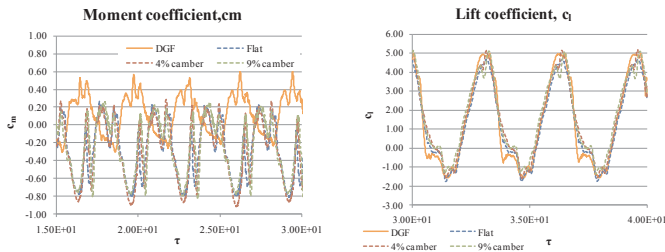


Fig. 18 (left) Moment coefficient ($Re = 2400$), Fig. 19 (right) Lift coefficient ($Re = 2400$)

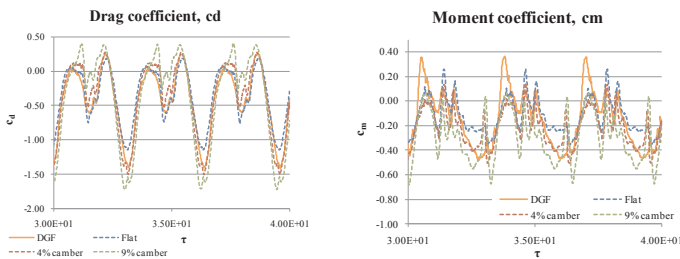


Fig. 20 (left) Drag coefficients ($Re = 2400$), Fig. 21 (right) Moment coefficient ($Re = 2400$)

	cl	cd	cm
DGF	1.607	-0.473	-0.215
Flat Plate	1.343	-0.420	-0.146
4% camber	1.677	-0.446	-0.247
9% camber	1.745	-0.422	-0.344

Table 4 Mean values of cl, cd and cm ($Re = 2400$)

With regard to lift coefficients, there cannot be seen any significant difference between the four tested airfoils. In addition, unlike the previous case, the four wings behave much in the same manner with regard to drag coefficients too, qualitatively. Regarding moment coefficients, however, the corrugated wing exhibits the largest deviation in value, opposite to the previous case, through the mean value remains fairly small. What is found most interesting here is that the corrugated wing yields the largest negative drag coefficient, that is to say, it likely transforms lift into thrust.

On top of the periodical fluctuation related to the flapping and feathering motions, there can be seen unsteady fluctuations in the diagrams of drag and moment coefficients. These are conceivably caused by vortices which are shed from the wing surface. This theory is underpinned by Figs. 24-27, which present the pressure distribution around the corrugated wing.

It can be confirmed from the diagrams that the corrugated wing releases a series of vortices from around the leading

edge (leading edge vortex, or LEV) on the upper surface

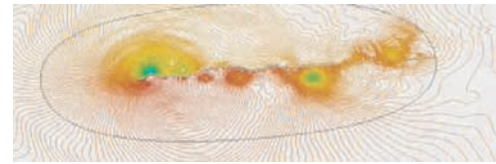


Fig. 22 Isobaric contours around the corrugated wing at the beginning of downstroke.

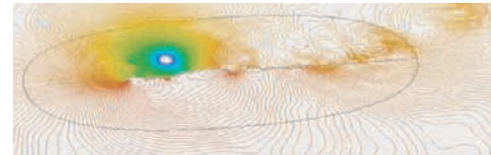


Fig. 23 Isobaric contours around the corrugated wing in the middle of downstroke.

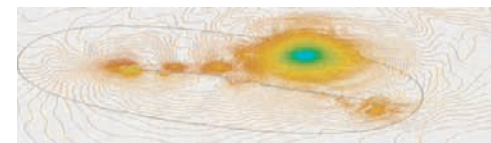


Fig. 24 Isobaric contours around the corrugated wing at the beginning of upstroke.



Fig. 25 Isobaric contours around the corrugated wing in the middle of upstroke.

during downstroke (Figs. 23 and 24). Also during upstroke, there can be seen LEV formed on the lower surface (Figs. 22 and 25), though they are much weaker than those seen on the upper surface during downstroke. Note that the same simulation was carried out for $Re = 7600$ as well but the wings behave much in the same way and thus the results shall be herein left out for want of space of paper.

4.0 DISCUSSION

This study shed light upon the aerodynamic properties and behaviours of a corrugated wing in low-Reynolds number flows by a CFD method. The stability against unsteady fluctuation of the corrugated wing spotted in Cases 1 and 2 may be the key to elucidate the mechanism of how insects can so stably fly. Such fluctuations are chiefly caused by vortices released from the wing surface, and corrugated wings can arguably seize vortices tight inside the concave rumples of its upper and lower surfaces, resulting in stabilising and smoothing the flow to exhibit small fluctuations in aerodynamic coefficients. This is quite likely, both theoretically and intuitively, and the visualised streamlines in this study actually reinforce this conjecture. During the unsteady test case of heaving and feathering motions in combination, the visualised streamlines from the present numerical simulation (Figs. 24-28) indicate that vortices shed from around the leading edge should be

playing a vital role in producing lift, moment, drag and unsteady fluctuations in their values. In fact, leading edge vortices are believed to be the key to understand low-Reynolds number aerodynamics^[6,7,8], and this study arguably captured the behaviours of leading edge vortices well.

The corrugated wing shows significant phase lags in drag and moment coefficients behind other three wings in Cases 3 to 6. This phase lag can also likely be attributed to the ability of the wing to retard vortices to come off, owing to its ruffled surface. However, the relationship (ideally both qualitatively and quantitatively) between the corrugated surface and vortices in terms of the strength of vortices, frequency of shedding vortices, angle of attack, wing profile, Reynolds number, stall angle, the stability of the wing in a low-Reynolds number flow and so on, remained unrevealed within the scope of this study. It can thus be a challenging future research topic to further clarify aerodynamic properties of corrugated wings in details.

Regarding Cases 5 and 6, the phase difference given between the heaving and feathering motions in this study is 90°, but this is only an example of possible combinations. As a matter of fact, it is pointed out that the optimal phase difference depends on flight condition^[9,10] and hence the most favourable combination of the two motions must be further studied^[11,12,13]. The numerical results obtained from this study fairly agree with experimental data of Ref. [1] in general, though nominal values of aerodynamic coefficients appear different due to the difference in non-dimensionalisation. The difference in the computational results from experimental data may partly be attributed to the fact that this study is based on the two-dimensional assumption. Three-dimensional modelling of a corrugated wing and its simulation can thus be a good future research topic to follow.

5.0 CONCLUSION

Conclusive remarks obtained from the present study can be summarised as follows;

- A remarkable stability of the corrugated wing against unsteady fluctuations in steady flows (in Cases 1 and 2) was spotted whilst the angle of attack is less than about 8°;
- Numerical results simulated in this study fairly agree with Obata's experimental data in general^[1];
- In Cases 3 and 4, the corrugated wing exhibits the smallest deviations both in drag and moment coefficients. This may indicate that the corrugated wing is most stable in heaving motion;
- In Cases 3 - 6, the phase of fluctuation in moment coefficient of the corrugated wing is obviously different from other three wings. The phase lag can arguably be attributed to the corrugatedness of the wing surface

and its influence upon vortex behaviours;

- In Cases 5 and 6, significantly advantageous aspects were not identified in any wings. Still, the phase lag in moment coefficient of the corrugated wing is conspicuous.

6.0 REFERENCES

1. Obata, A. and Sinohara, S., "Flow Visualization Study of the Aerodynamics of Modeled Dragonfly Wings," *AIAA Journal*, Vol. 47, No. 12, Dec. 2009, pp. 3043-3047
2. Okamoto, M. and Azuma, A., "Experimental Study on Aerodynamic Characteristics of Unsteady Wings at Low Reynolds Number," *AIAA Journal*, Vol. 43, No. 12, pp.2526- 2536, Dec. 2005
3. Tanabe, Y., Saito, S. and Otani, I., "Application of SLAU Scheme to Helicopter CFD," 41st Fluid Dynamics Conference/Aerospace Numerical Simulation Symposium 2009, Chofu, Tokyo, June 18-19 2009 (In Japanese.)
4. Shima, E. and Kitamura, K., "On New Simple Low-Dissipation Scheme of AUSM-Family for All Speeds," 47th AIAA Aerospace Sciences Meeting, AIAA Paper 2009-136, Orlando, FL, January 5-8 2009.
5. Wang, Z.J., "Vortex shedding and frequency selection in flapping flight," *J. Fluid Mech.* Vol. 410, pp.323-341, 2000
6. Ellington, C.P., "Insects versus Birds: The Great Divide," AIAA Paper 2006-35, 2006
7. Okamoto, M. and Jinba, Y., "Experimental Study on Aerodynamic Characteristics of Wing Planforms at Low Reynolds Number," bulletin paper of Akita National College of Technology, pp.42-50, 2009 (In Japanese)
8. Hart, A. and Ukeiley, L., "Low Reynolds Number Unsteady Aerodynamics over a Pitching-Plunging Flat Plate," AIAA Paper 2010-387, 2010
9. Isogai, K., Kamisawa, Y. and Sato, H., "Resonance Type Flapping Wing for Micor Air Vehicle," *Trans. Japan Soc. Aero. Space Sci.* Vol. 52, No. 127, pp.199-205, 2010
10. Kamisawa, Y. and Isogai, H., "Study on Optimum Flapping Wing Motions of Dragonfly," *Trans. Japan Soc. Aero. Space Sci.* Vol. 51, pp.114-123, 2008
11. Ansari, S.A., Knowles, K. and Zbikowski, R., "Insectlike Flapping Wings in the Hover Part 1: Effect of Wing Kinematics," *Journal of Aircraft*, Vol. 45, No.6, Nov.-Dec., 2008
12. Ansari, S.A., Knowles, K. and Zbikowski, R., "Insectlike Flapping Wings in the Hover Part 2: Effect of Wing Geometry," *Journal of Aircraft*, Vol. 45, No.6, Nov.-Dec., 2008
13. Rosenfeld, N. C. and Wereley, N. M., "Time-Periodic Stability of a Flapping Insect Wing Structure in Hover," *Journal of Aircraft*, Vol. 46, No. 2, Mar.-Apr., 2009